


# Studying crystallisation processes using electron microscopy: The importance of sample preparation

Martha Ilett<sup>1</sup>  | Maryam Afzali<sup>1</sup> | Bilal Abdulkarim<sup>1</sup> | Zabeada Aslam<sup>1</sup> |  
Stephanie Foster<sup>1</sup> | Miguel Burgos-Ruiz<sup>2</sup> | Yi-Yeoun Kim<sup>3</sup> | Fiona C. Meldrum<sup>3</sup> |  
Rik M. Drummond-Brydson<sup>1</sup>

<sup>1</sup>School of Chemical and Process Engineering, University of Leeds, Leeds, UK

<sup>2</sup>Department of Mineralogy and Petrology, University of Granada, Granada, UK

<sup>3</sup>School of Chemistry, University of Leeds, Leeds, UK

## Correspondence

Martha Ilett, School of Chemical and Process Engineering, University of Leeds, Leeds, LS2 9JT, UK.  
Email: [m.a.ilett@leeds.ac.uk](mailto:m.a.ilett@leeds.ac.uk)

## Funding information

Engineering and Physical Sciences Research Council, Grant/Award Numbers: EP/R018820/1, EP/M028143/1; University Of Leeds; Wellcome, Grant/Award Numbers: 108466/Z/15/Z, 221524/Z/20/Z

## Abstract

We present a comparison of common electron microscopy sample preparation methods for studying crystallisation processes from solution using both scanning and transmission electron microscopy (SEM and TEM). We focus on two widely studied inorganic systems: calcium sulphate, gypsum ( $\text{CaSO}_4 \cdot 2\text{H}_2\text{O}$ ) and calcium carbonate ( $\text{CaCO}_3$ ). We find significant differences in crystallisation kinetics and polymorph selection between the different sample preparation methods, which indicate that drying and chemical quenching can induce severe artefacts that are capable of masking the true native state of the crystallising solution. Overall, these results highlight the importance of cryogenic (cryo)-quenching crystallising solutions and the use of full cryo-TEM as the most reliable method for studying the early stages of crystallisation.

## KEYWORDS

crystallisation, electron microscopy, sample preparation

## 1 | INTRODUCTION

Improving our understanding of crystallisation is crucial for controlling the production of ceramics, pharmaceuticals, fine chemicals, nanomaterials and biominerals.<sup>1–3</sup> Equally important is the prevention of unwanted weathering caused by crystallisation, and the formation of scale or kidney stones.<sup>4,5</sup> Despite the importance of crystallisation, we still have a poor understanding of many of the mechanisms that underlie this fundamental phenomenon.<sup>6</sup> This is due to the fact that crystallisation is governed by molecular scale processes that can be extremely fast, which make it very difficult to study experimentally.<sup>6–10</sup>

It is now widely recognised that many crystalline materials form via nonclassical nucleation and growth mechanisms.<sup>11</sup> Electron microscopy is a powerful tool for studying the early stages of crystallisation processes and to ascertain the exact mechanisms in operation. A key issue is to ensure that samples are studied in their native state and are representative of the species and structures involved in crystallisation from solution, or potentially from the gas phase. In this study, we focus exclusively on crystallisation in aqueous solutions, which can be influenced by factors including supersaturation, temperature, pressure, solvent composition, impurities/ seeds and confinement.

This is an open access article under the terms of the [Creative Commons Attribution](https://creativecommons.org/licenses/by/4.0/) License, which permits use, distribution and reproduction in any medium, provided the original work is properly cited.

© 2024 The Authors. *Journal of Microscopy* published by John Wiley & Sons Ltd on behalf of Royal Microscopical Society.

Historically, crystallising solutions were prepared for examination using scanning electron microscopy (SEM) or transmission electron microscopy (TEM) by simply drop casting a droplet of the crystallising solution onto a sample stub (SEM) or a support film (TEM) and drying in air. However, drying can induce nonuniform particle deposition and particle aggregation, in addition to increasing progressively the solute concentration in the solvent.<sup>12</sup> A variation of this approach is to rapidly remove the solvent via vacuum filtration onto a filter paper or TEM support film.<sup>13</sup> Another option is to chemically quench crystallisation via the addition of a suitable reagent (such as an alcohol) to either the droplet or the bulk solution, although this can alter the activity of water and affect the crystallisation pathway in aqueous systems.<sup>14</sup>

Our group and others have previously used cryogenic (cryo-) TEM to study crystallisation processes and have shown that this offers substantial benefits over conventional drying techniques for TEM sample preparation.<sup>15,16</sup> Principally, rapid freezing of the sample entraps it within vitreous ice in a state analogous to that in solution. In this frozen state it is possible to perform detailed analysis at individual reaction times. Cryo-TEM also has benefits over in situ liquid phase TEM in that electron beam effects are reduced due to the lower temperatures in cryo-TEM reducing radiolytic reaction rates and also owing to the limited diffusion of reactive radiolytic products in ice compared to water, additionally confinement effects are effectively eliminated.<sup>15–18</sup>

This work focuses on the crystallisation of two inorganic systems from aqueous solution: calcium sulphate and calcium carbonate. Calcium sulphate is important in both environmental and engineering contexts and exists as anhydrite ( $\text{CaSO}_4$ ), bassanite ( $\text{CaSO}_4 \cdot 0.5\text{H}_2\text{O}$ ) and gypsum ( $\text{CaSO}_4 \cdot 2\text{H}_2\text{O}$ ). Gypsum is the most stable phase under ambient conditions, while anhydrite becomes stable above ca. 60°C. Bassanite is unstable with respect to anhydrite and gypsum but precipitates from solution at temperatures above ca. 90°C due to the slow kinetics of anhydrite formation.<sup>19</sup> Bassanite has been reported to form in water/alcohol mixtures and is also stabilised in confinement.<sup>20–22</sup> Significant efforts have been made to determine the mechanism through which calcium sulphate precipitates and these are highlighted in our previous publication.<sup>15</sup> Specifically, earlier literature suggests that gypsum forms via a two-step process, while more recent publications suggest that an amorphous precursor forms during the precipitation of gypsum.<sup>20,23–25</sup> Further reports also suggest that a nonclassical mechanism occurs in which a bassanite intermediate self-assembles and undergoes a solid-state transformation to gypsum.<sup>26,27</sup>

In turn, calcium carbonate is highly important in many natural processes such as sedimentation and scaling and

has also found numerous applications as an additive and filler in many industrial products. It can exist in many different forms: amorphous calcium carbonate (ACC), two hydrated polymorphs and three anhydrous forms. The hydrous forms, monohydrate calcite (MHC) and calcium carbonate hexahydrate (ikaite), are generally only formed under relatively extreme conditions.<sup>15,28</sup> The anhydrous polymorphs naturally occur as three major species. Calcite is the most thermodynamically stable phase typically displaying a rhombohedral habit. Aragonite crystals are thermodynamically less stable than calcite, have an orthorhombic symmetry, and typically exhibit acicular morphologies.<sup>29</sup> Vaterite is a metastable phase, which often appears as an intermediate between ACC and calcite or aragonite and usually forms spherical, polycrystalline particles.<sup>30,31</sup>

ACC often forms as a precursor to the anhydrous polymorphs in aqueous solution and exists as spherical nanoparticles with composition  $\text{CaCO}_3 \cdot x\text{H}_2\text{O}$ , with  $x$  in the range 1 to 1.5.<sup>32,33</sup> Nucleation of ACC has been suggested to proceed via the association of stable, pre-nucleation clusters (PNCs) in solution, which undergo an intermediate step of liquid–liquid phase separation (LLPS), although the existence of PNCs has been disputed by others.<sup>34,38</sup> LLPS occurs when the local liquid composition fluctuates and crosses the binodal limit for demixing into two distinct liquid phases containing different amounts of dissolved cations and anions (i.e. solute-rich and solute-poor phases). Further dehydration of the dense liquid phase (DLP) is suggested to result in the formation of 10–20 nm hydrated ACC particles that have been proposed to possess a short range order reminiscent of the anhydrous phases, referred to as its proto-structure.<sup>35</sup>

The current work compares and contrasts a number of different common sample preparation routes for studying the aqueous crystallisation of calcium sulphate and calcium carbonate. We find significant differences in the observations from the different preparation routes, then rationalise these and determine the optimum method for assessing the ‘native state’ of the crystallising solution. This will provide insight when designing EM experiments for studying crystallisation and ultimately allow us to exert a greater degree of control over crystallisation processes.

## 2 | RESULTS

The crystallisation of calcium sulphate and calcium carbonate were studied. For calcium sulphate 50 and 100 mM calcium sulphate solutions were prepared by mixing 100 mM calcium chloride and sodium sulphate solu-

tions. For calcium carbonate, 4.5 mM calcium carbonate solutions were prepared by mixing 9 mM calcium chloride and sodium carbonate solutions. Both systems were then analysed by SEM and TEM at specified time points. Samples were prepared from solution by one of five different methods: (i) air drying at ambient temperatures; (ii) vacuum filtration; (iii) chemical quenching using ethanol; (iv) cryogenic quenching followed by vacuum sublimation of the vitreous ice (and room temperature observation); and finally (v) cryogenic quenching and observation by cryo-TEM. See Section 5 for more details.

## 2.1 | Calcium sulphate

### 2.1.1 | Samples prepared by drying

No significant differences were observed between samples prepared via air drying or vacuum filtering. Both bassanite and gypsum crystals were observed in a 50 mM  $\text{CaSO}_4$  solution after 20 min, as identified by their morphologies and confirmed by selected area electron diffraction (SAED). Bassanite crystals presented as aggregates of small nanorods in a 'sheaf'-like morphology, measuring  $0.95 \pm 0.28 \mu\text{m}$  for air-dried samples (Figures 1A and S2) and  $2.4 \pm 1.0 \mu\text{m}$  for vacuum-filtered samples (Figures 1D and S3). Often these aggregates had an associated NaCl crystal attached to them, which we assume had nucleated heterogeneously on the bassanite sheaf (Figures S2 and S3). Gypsum crystals were observed with multiple morphologies, with a maximum Feret diameter of  $4.0 \pm 1.1 \mu\text{m}$  for air-dried samples (Figures 1B and S2) and  $5.3 \pm 2.6 \mu\text{m}$  for vacuum-filtered samples (Figures 1D and S3). Samples were taken at two further time points (1 and 5 min) and no significant differences were observed (Figures S4 and S5). Similarly, 100 mM  $\text{CaSO}_4$  samples were prepared with no notable changes in experimental observations as compared to the 50 mM solution.

### 2.1.2 | Samples prepared by chemical quenching in ethanol

Ethanol was used to chemically quench the crystallisation of 50 mM  $\text{CaSO}_4$  solutions after 20 min of reaction. In this instance almost all the observed crystals were bassanite (Figures 1E and S6). A higher number of bassanite crystals were observed than in the dried samples and the morphology of the bassanite was very different; here the bassanite nanorods appeared as individual crystals with no evidence of the sheaf-like bassanite previously seen after air drying/vacuum filtering. The bassanite nanorods var-

ied in size from 100 nm up to  $1.5 \mu\text{m}$  (mean size  $380 \pm 310 \text{ nm}$ ) and large gypsum crystals were observed albeit in smaller numbers than in air-dried or vacuum-filtered samples (Figure 1F). Again, no significant differences were observed at higher concentrations (100 mM) or longer time points (2 h) (Figure S7).

### 2.1.3 | Samples prepared by cryogenic quenching

Samples prepared by cryogenic quenching and vacuum sublimation of 50 mM  $\text{CaSO}_4$  solutions after 5 and 20 min did not show any evidence of bassanite or gypsum crystals (Figure 2). However, small amorphous particles were observed, which energy dispersive X-ray (EDX) analysis showed were rich in calcium and sulphur (Figure 2D and F). This is indicative of an amorphous calcium sulphate (ACS) species, although we note the morphologies of these particles were nonspherical. These were of the order of 100 nm in diameter and uniformly distributed throughout the TEM grid (Figure 2A and C). In addition to the presence of the ACS regions, there was extensive precipitation of NaCl crystals (Figure 2B – see later comments in Section 3.2). At higher concentrations of 100 mM  $\text{CaSO}_4$ , gypsum crystals (alongside NaCl and other solute hydrates) were observed after 20 min (Figure S8), with no evidence of bassanite crystals.

Cryogenically quenched samples that were examined at low temperature using cryo-TEM did not reveal any crystals at a concentration of 50 mM. However, gypsum crystals were observed within the vitreous ice, at 100 mM solutions but only after a time period of 2 h (Figure 3). The lack of crystals observed at 50 mM and shorter time points could have been due to the fact that any crystals were too small to resolve within the ice, or that there were few crystals in solution such that they were very sparsely populated on the TEM grid, a problem common to cryo-TEM sample preparation.

## 2.2 | Calcium carbonate

### 2.2.1 | Samples prepared by drying

As in the case of calcium sulphate, calcium carbonate samples prepared via either air drying or vacuum filtering were similar. For the air-dried samples, after 5 min reaction time, TEM showed the presence of spherical ACC particles with a mean size of  $215 \pm 112 \text{ nm}$  (Figures 4A and S9A) as well as polycrystalline vaterite and rhombohedral calcite crystals  $\sim 1\text{--}2 \mu\text{m}$  in dimension (Figures 4B and S9B). After 15 min, SEM images revealed larger ACC

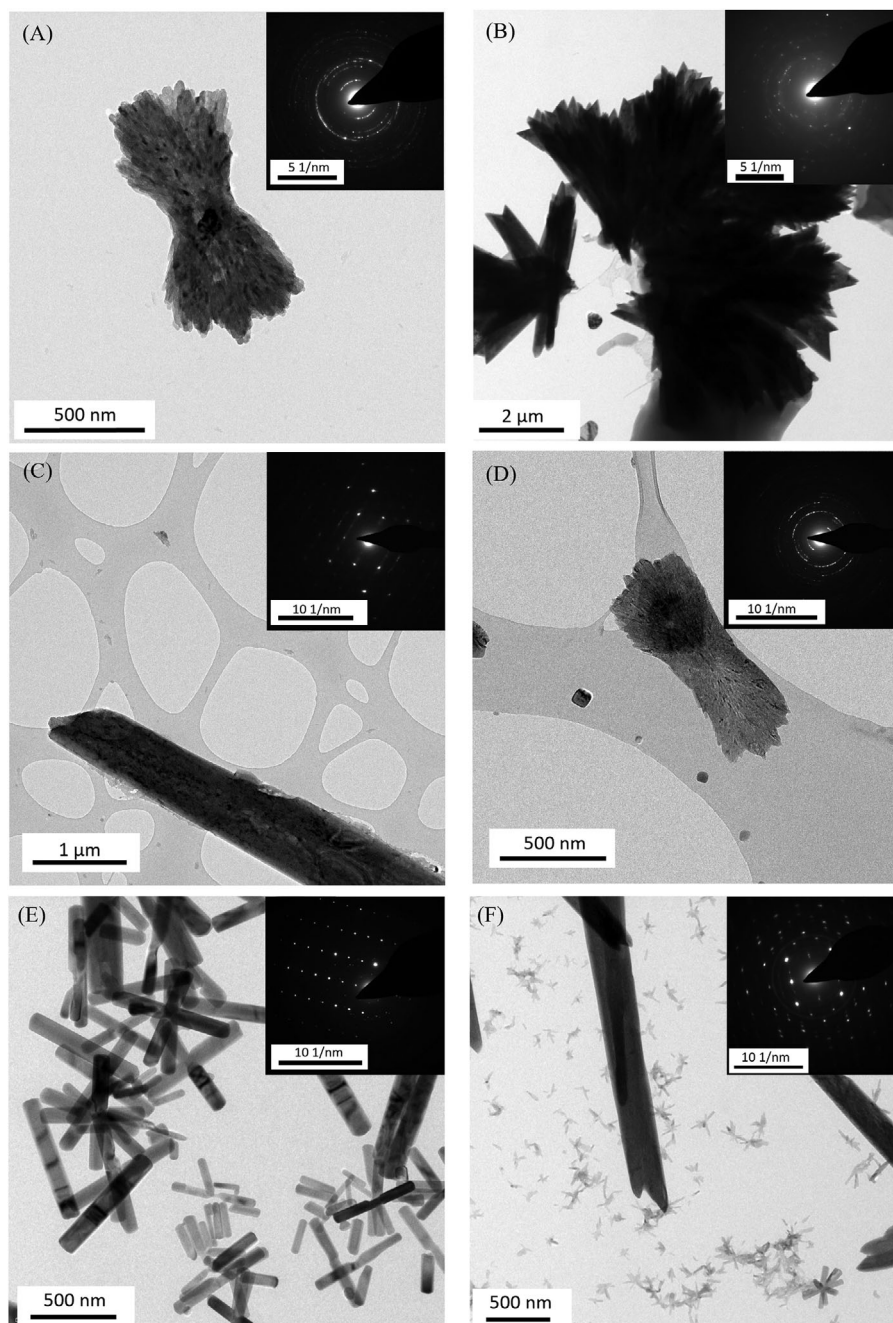


**FIGURE 1** TEM images alongside SAED patterns taken from a 50 mM CaSO<sub>4</sub> solution prepared via mixing CaCl<sub>2</sub> and Na<sub>2</sub>SO<sub>4</sub> for 20 min. Samples were prepared for TEM analysis via air drying (A, B), vacuum filtering (C, D) and ethanol quenching (E, F). For air drying and vacuum filtering, there were no significant differences in the crystals observed. Both bassanite and gypsum crystals were seen and bassanite crystals were aggregated in a sheaf-like morphology (A, D) while gypsum crystals appeared as both individual crystals (C) and aggregated crystals (B). Samples prepared via ethanol quenching were markedly different to air-dried/vacuum-filtered samples with predominantly single crystal nanorod shaped bassanite observed (E), with just a few larger individual gypsum crystals seen (F). All SAED patterns confirmed either bassanite or gypsum crystal phase; for larger fitted patterns, see Figure S1.

particles of  $325 \pm 108$  nm and larger vaterite and calcite crystals (Figure S9C–E). After 40 min, vaterite and calcite had aggregated into larger particles  $\sim 5$ – $20$  μm in dimension, but there was no evidence of ACC (Figure S9F and G). This suggests that all ACC had transformed to crystalline structures.

After 5 min of reaction, vacuum-filtered samples contained ACC particles with diameters of  $335 \pm 117$  nm and calcite particles that were 450–750 nm in size (Figures 4C and D and S10A and B). The precipitates observed by TEM after 15 min were ACC ( $337 \pm 137$  nm in size), vaterite and calcite with a size range of 0.7–10 μm (Figure S10C and D).



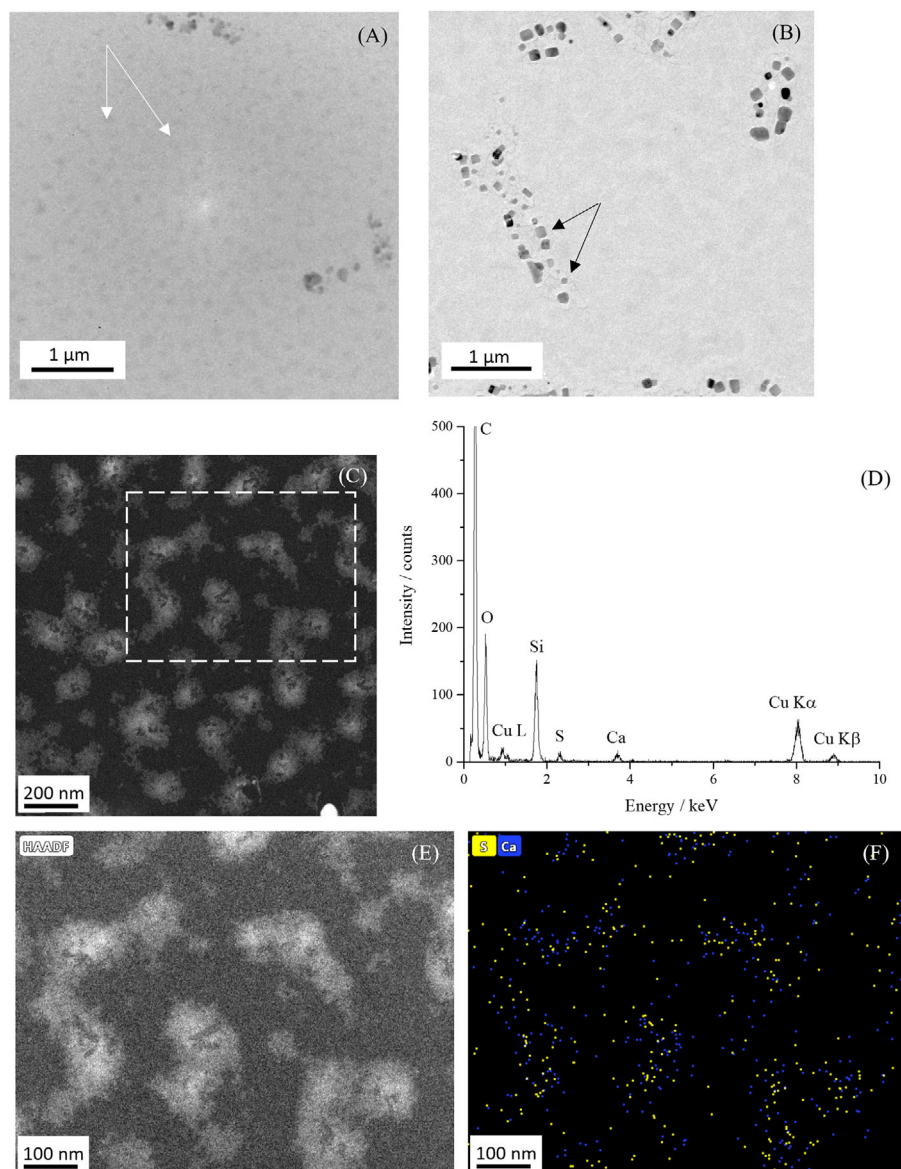


**FIGURE 2** SEM/TEM analysis of 50 mM  $\text{CaSO}_4$  solutions cryo-quenched after 5 min and then brought up to room temperature via controlled warming under vacuum. No bassanite or gypsum crystals were observed, but amorphous Ca- and S-rich particles were observed (white arrows in A) alongside NaCl crystals (black arrows in B). High angle annular dark field (HAADF) scanning TEM (STEM) of the amorphous features is shown in C alongside STEM EDX analysis of the dashed box in C (HAADF image (E)), which showed Ca and S K-X-ray signals (D) that spatially resolved to the amorphous particles (F).

After 40 min, again only calcite and vaterite (size range  $\sim 0.7\text{--}12\text{ }\mu\text{m}$ ) were observed (Figure S10E and F).

## 2.2.2 | Samples prepared by chemical quenching in ethanol

For samples prepared by ethanol quenching, two distinct ACC morphologies were observed after 5 min of reaction: isolated, individual ACC particles between  $250 \pm 110\text{ nm}$  in size and extended networks of smaller ( $32 \pm 17\text{ nm}$ ) ACC particles (Figures 4E and S11B). Interestingly, only ethanol

quenching led to the formation of these extended ACC networks on the TEM grid. TEM also revealed the presence of aggregated calcite crystals after 5 min of reaction (Figures 4F and S11A) as confirmed by electron diffraction. After 15 min reaction time, SEM revealed that the dimensions of both the individual ACC particles ( $278 \pm 85\text{ nm}$ ) and clusters of ACC particles ( $40 \pm 30\text{ nm}$ ) had increased, and a greater number of vaterite and calcite crystals were observed (Figure S11C and D). As for the dried samples, ACC was not observed after 40 min of reaction and only aggregated vaterite and calcite crystals were identified (Figure S11E and F).

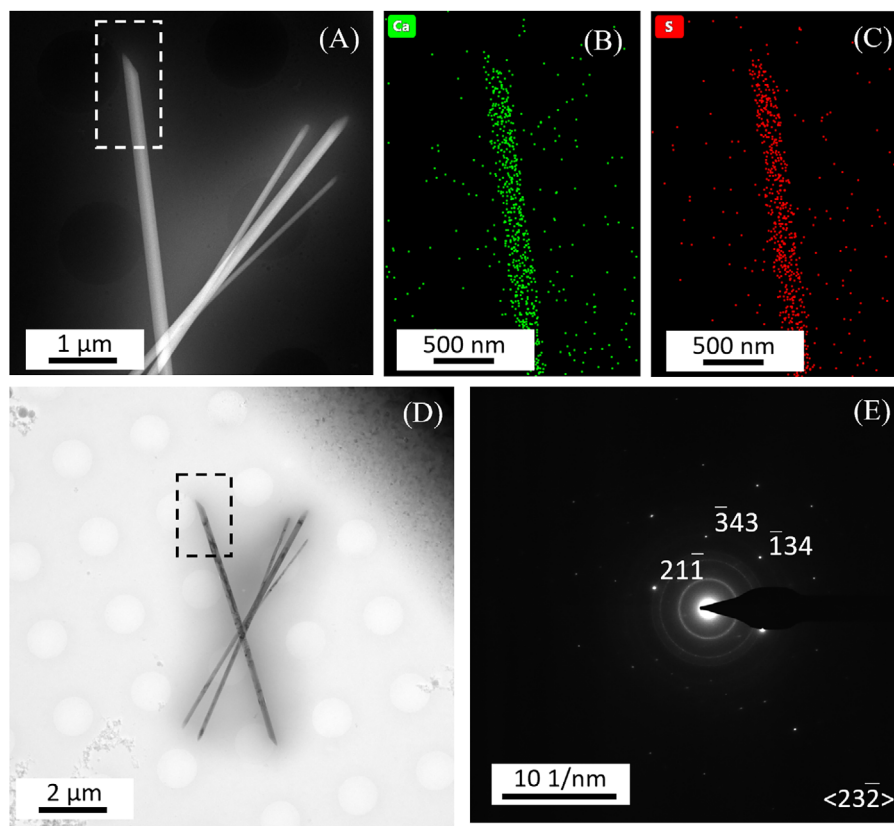


**FIGURE 3** S/TEM analysis of a 100 mM  $\text{CaSO}_4$  solution taken after 2 h of mixing  $\text{CaCl}_2$  and  $\text{Na}_2\text{SO}_4$  solutions. Only large gypsum crystals were observed (A, D) with no evidence of bassanite crystals on the TEM grid. HAADF STEM EDX confirms crystals were Ca and S rich (B, C) and SAED patterns indexed to gypsum (E).

### 2.2.3 | Samples prepared by cryogenic quenching

Only ACC and NaCl crystals were observed in samples prepared via cryogenic quenching and vacuum sublimation, after 5 to 15 min of reaction. The size range of the ACC particles increased from  $105 \pm 150$  nm after 5 min (Figure 5A) to  $395 \pm 117$  nm after 15 min, and no crystalline calcium carbonate could be clearly identified. After 40 min, SEM micrographs showed ACC particles in the size range  $403 \pm 80$  nm. The surface morphologies of these particles had changed with respect to the ACC particles observed after 5 min of reaction (Figure 5B), perhaps suggesting that the ACC particles were potentially dissolving, or that a phase transformation from an amorphous structure to a crystalline structure was taking place.

Cryogenically quenched samples examined at low temperature using cryo-TEM were very different to samples prepared by other methods, in particular drying/filtering and chemical quenching. After a crystallisation time of 5 min, cryo-TEM images showed the presence of  $376 \pm 112$  nm nano-sized spherical ACC particles (Figure 5C). In

addition, micron-sized dark regions were evident in bright field images that possessed diffuse boundaries and contrasted with the surrounding vitreous ice. SAED patterns of these dark, diffuse regions confirmed that they were amorphous (Figure 5C, inset). ACC particles persisted after 15 min ( $285 \pm 90$  nm) and after 40 min had aggregated into  $353 \pm 115$  nm clusters with evidence of calcite formation (Figure 5D). In addition, a small number of calcite crystals were observed at all timepoints and confirmed via SAED (Figures 5D and S12).

## 3 | DISCUSSION

### 3.1 | Rationalisation of results

The fact that the outcomes of both sets of TEM experiments, and hence any conclusions drawn on the crystallisation mechanisms involved, are highly dependent on the sample preparation method is a key finding of this work. This has major implications for previous literature reports on the crystallisation of both calcium sulphate and calcium carbonate. A table summarising all the results

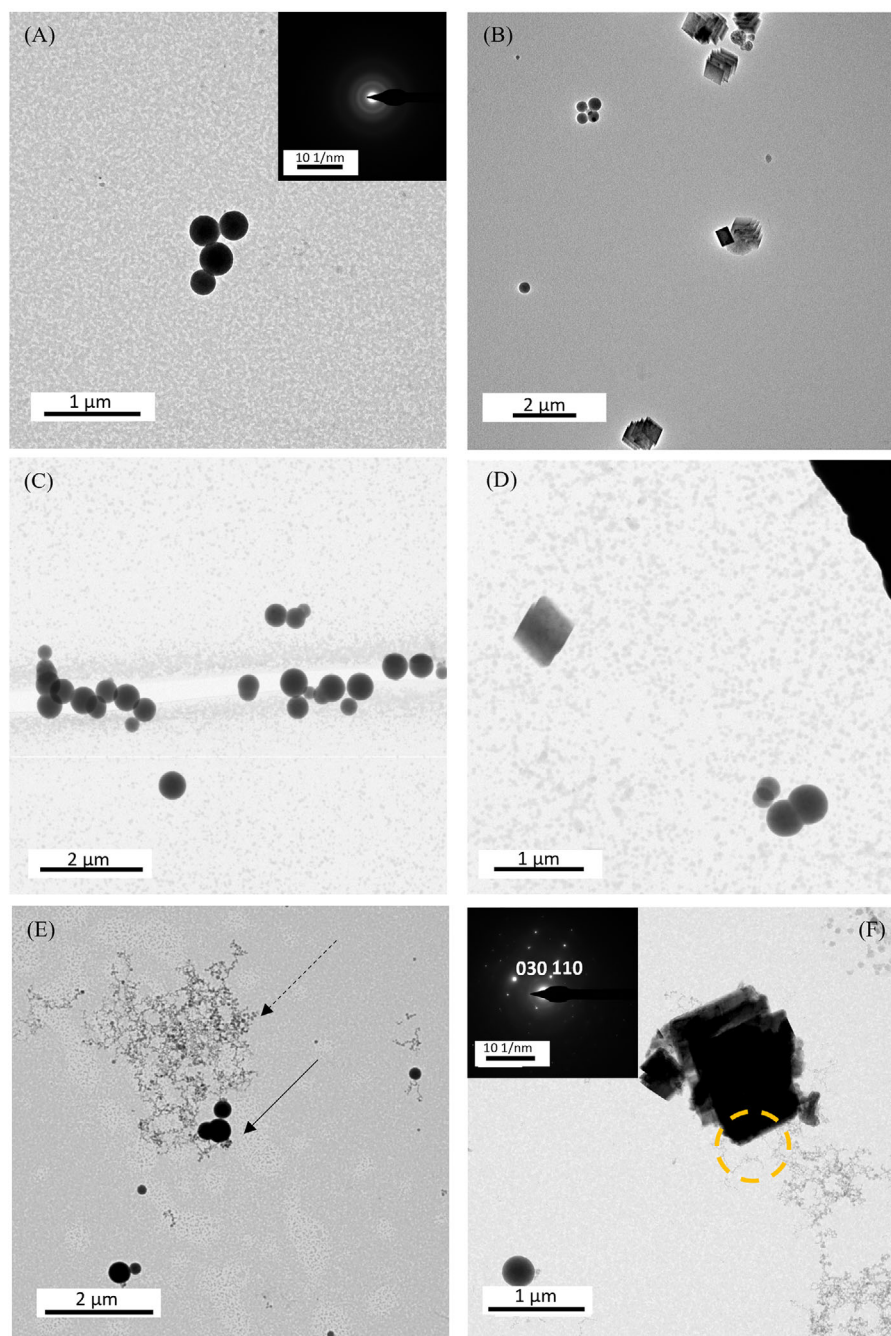


**FIGURE 4** TEM images and SAED patterns from 4.5 mM crystallising solutions of  $\text{CaCO}_3$  after 5 min mixing and prepared via one of three methods. (A, B) Samples prepared via air drying showed evidence of both ACC (SAED inset in A) and crystalline calcite and vaterite. (C, D) Samples prepared via vacuum filtering showed no significant difference from air drying with ACC and crystallites of  $\text{CaCO}_3$  observed. (E, F) Samples prepared via ethanol quenching were very distinct with ACC occurring as either individual particles (solid arrow in E) or extended networks of smaller ACC particles (dashed arrow in E); again crystallites were still observed after 5 min (F) with inset SAED of circled area indexing to calcite.

and artefacts of the different TEM sample preparation methods can be found in the SI (Table S1); however, the distinct differences for the two chemical systems may be rationalised as below in Sections 3.1.1 and 3.1.2.

In general terms, there has to be a thermodynamic driving force for crystallisation of a particular species

to occur; that is, the saturation index for a particular species or polymorph has to be positive. The saturation index for a particular species/polymorph varies as a function of both supersaturation and temperature. However, the kinetics of the nucleation process are separate, and the rate of crystallisation depends on height of the



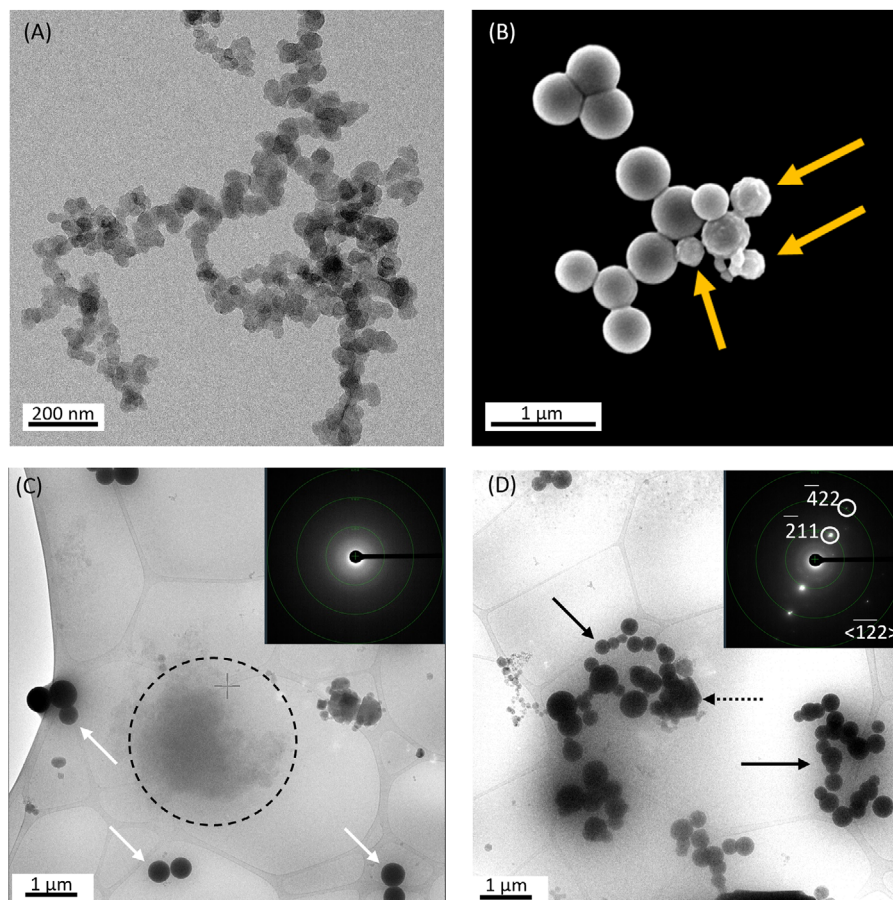


**FIGURE 5** Samples prepared at 4.5 mM via cryo-quenching and (A) controlled warming under vacuum after 5 min of reaction, (B) controlled warming under vacuum after 40 min of reaction, (C) full cryo-imaging after 5 min and (D) full cryo-imaging after 40 min. For samples prepared via cryo-quenching and controlled warming under vacuum, after 5 min, only ACC was observed, while after 40 min, ACC was also observed but in addition there was evidence of dissolution and/or crystallisation of these ACC particles (yellow arrows in (B)). For samples prepared via cryo-quenching and full cryo-imaging, after 5 min, regions of higher contrast were seen (dashed circle in C), which were confirmed as amorphous through SAED (inset in C) alongside ACC particles (white arrows in C). After 40 min of reaction, both ACC (black arrows in D) and calcite particles (dashed black arrow in D) were observed; the SAED pattern inset in D corresponds to the crystalline region highlighted by the dashed black arrow in D, which illustrates crystalline particles are present that index to calcite crystals.

free energy barrier for nucleation. Once nucleation has occurred then a stable nucleus can grow via addition of species from solution and/or transform to another species/polymorph.

### 3.1.1 | Calcium sulphate

At a  $\text{CaSO}_4$  concentration of 50 mM, the solution is supersaturated with respect to gypsum but not to bassanite; the saturation indices at 21°C have been calculated to be 0.50 and  $-0.37$  for gypsum and bassanite respectively.<sup>26</sup> However, the SI of bassanite becomes positive a little above 100 mM and so any form of drying will increase the supersaturation and, from a thermodynamic perspective, cause bassanite to precipitate alongside gypsum. This suggests that once it becomes thermody-

namically favourable to nucleate bassanite, the nucleation rate and/or induction time is relatively fast compared to that of gypsum and further bassanite nucleates heterogeneously on this existing bassanite to form sheaf-like aggregates.

Chemical quenching in ethanol can rapidly alter the activity of water and change the dielectric constant of the medium, which in turn impacts interionic attraction and solute-solvent interactions. The presence of ethanol favours the formation of bassanite over gypsum, and instead of forming sheaf-like aggregates, bassanite homogeneously nucleates throughout the solution leading to isolated nanorods. This has been noted before by Yang et al. and Tritschler et al.<sup>36,22</sup> The latter study reported that a water:ethanol mix of < ca. 40 wt% (ca. 60 mol%) of water relative to ethanol strongly favours the formation of bassanite over gypsum. As mentioned by van Driessche, we



can infer that ethanol quenching either promotes bassanite, potentially by withdrawing water from either liquid or amorphous precursors, or stabilises it from transformation to the dihydrate gypsum.<sup>19</sup>

We note that bassanite was absent in cryogenically quenched samples, and that gypsum was the only phase observed. Precipitation occurred at longer times suggesting that the kinetics of gypsum crystallisation are relatively slow (on the order of hours) as compared to those of bassanite. Importantly, this suggests that bassanite is not involved as an intermediate in the direct formation of gypsum from 50 mM supersaturated solutions, although it could be that the intermediate clusters proposed by Stawski are too low in contrast to resolve within 100 nm of vitreous ice during cryo-TEM examination, or that any intermediate is extremely transient.<sup>26</sup> We note that while gypsum was evident in 100 mM samples in samples prepared by cryogenic quenching and vacuum sublimation, only amorphous calcium sulphate regions were observed in 50 mM samples. Interestingly these ACS species were not spherical, suggesting that they were not originally solid but instead could be remnants of a liquid-like precursor resulting from binodal liquid de-mixing within the solution.<sup>37</sup> This would explain the relatively noisy EDX maps presented in Figure 2F as these dense liquid regions would be expected to have originally incorporated significant amounts of solvent molecules, resulting in relatively low concentrations of both calcium and sulphur. This is expected to result in a discontinuous network of a solute-rich phase in a solute-poor matrix as is observed here (Figure 2). However, we note that there is no corroborating evidence in the literature for this phenomenon occurring in the calcium sulphate system and there remains the possibility that this occurs as a result of the cryogenic quenching and vacuum sublimation sample preparation. Yet in this case, one might expect to observe a more bi-continuous network, similar in form to spinodal decomposition and involving diffusion of species most probably during the slow vacuum sublimation step.<sup>37</sup>

### 3.1.2 | Calcium carbonate

Both air-drying and vacuum-filtration sample preparation methods resulted in morphologically similar  $\text{CaCO}_3$  particles. ACC particles were only observed within the first 15 min and vaterite and calcite were observed at all time points. As discussed for the case of calcium sulphate, both of these methods will lead to an increase in supersaturation, albeit at different rates. This shortens the lifetime of ACC particles as the driving force for crystallisation progressively increases. Conversely, there is no such increase in supersaturation in the cryogenic quench-

ing/vacuum sublimation method, and only ACC particles were observed after 5 and 15 min with no evidence of crystalline polymorphs. After 40 min, ACC particles were still observed but possessed a rough surface texture, which could be indicative of the potential transformation of ACC to crystalline polymorphs or dissolution. This was not observed using the drying/filtering methods and demonstrates that quenching/vacuum sublimation is a better sample preparation method for observing amorphous or metastable phases rather than drying, where these phases will have reduced lifetimes.

The full cryo-TEM study identified the formation of darker, disordered micron-sized regions with diffuse boundaries embedded within the vitrified solution after 5 min reaction time. These features are similar to those reported by Smeets et al. who suggested that these were evidence for a dense liquid-like phase (DLP) that is rich in solute ions and that forms through a binodal de-mixing process.<sup>38</sup> Based on our measured contrast difference between these dense regions and the surrounding vitreous ice and using a Beer–Lambert type expression for mass-thickness contrast, this implies an increased density of approximately 10% in these regions. We postulate that these features are precursors to the subsequent precipitation of ACC particles, which grow over time and eventually transform to calcite. These diffuse disordered structures may also have been present in the cryogenically quenched/vacuum sublimed samples, although we were unable to differentiate these from the background TEM support film.

Interestingly, Zou et al. have derived a phase diagram for calcium carbonate solutions as a function of concentration and temperature via SEM analysis of the observed size of ACC particles formed during the fast mixing of calcium chloride and sodium carbonate solutions.<sup>39</sup> Applying established theories of phase separation they predicted that the room temperature solution is unstable beyond a concentration of 3–4 mM of calcium and carbonate ions and will spontaneously precipitate ACC via spinodal decomposition. Below this spinodal limit, but above the solubility limit, they predict that the fluid mixture is metastable and can phase separate into a liquid rich in solvent and a liquid rich in solute (i.e. a dense liquid phase); at longer times, this dense liquid phase can potentially form a crystalline nucleus of composition close to the final one via thermal fluctuations and, if larger than the critical nucleus size, it can grow leading to a crystalline polymorph such as vaterite or calcite. This derived phase diagram fits well with our current cryo-TEM observations, in that at a concentration of 4.5 mM, we are above the spinodal line and observe the presence of both a dense liquid phase and ACC particles. At a lower supersaturation of 0.5 mM, we are in the metastable region and here we observe only the pres-

ence of a DLP which is significantly denser (approximately 20–30% denser than the surrounding vitreous ice based on a Beer–Lambert type analysis of cryo-TEM micrographs) than the DLP observed above the spinodal line, with no evidence for the formation of ACC particles at this lower supersaturation level (see Figure S13).

Finally, we note that it was only the ethanol quenching technique that resulted in the formation of an extended network of small ACC nanoparticles. One explanation could be that the dense liquid precursor formed by de-mixing was dehydrated by the ethanol. Ethanol is known to stabilise ACC and influence the crystalline polymorph produced.<sup>14,40,41</sup> Walker et al. observed the early stages of formation of an extended ACC network in mixed water/ethanol solvents, similar to the ACC networks observed in this work, which ultimately led to the formation of aragonite after 1 h.<sup>41</sup> Similar ACC networks have also been observed in the study of ACC (pseudo)-poly-amorphism (so called proto-calcite, proto-vaterite and proto-aragonite structured ACCs) dependent on pH and temperature.<sup>42</sup> However, they used an ethanol quench to arrest the reaction which, on the basis of our findings, could have led to artefactual results. The addition of ethanol will lead to a rapid alteration in the activity of water and change levels of supersaturation, which may lead to the apparent differences in kinetics. We also note that in the work of Zou et al., they used a (cold) ethanol quench and rapid vacuum filtration of crystallising solution, followed by examination of the powders by SEM.<sup>39</sup> However, they did not report the network of small (tens of nm diameter) ACC particles, which we observe following ethanol quenching, instead they only identified the larger (hundreds of nm diameter) ACC particles. We believe that this could have been due to either the resolution of the SEM imaging and/or the transfer of the dried powder onto the SEM stub.

### 3.2 | Implications for the study of crystallisation processes using electron microscopy

This study clearly reveals that when aqueous crystallisation processes are studied by electron microscopy, sample artefacts can be induced by air drying, vacuum filtration and chemical quenching of the crystallisation solutions.

Cryogenic quenching presents a more faithful representation of the solute species present in the solution at a given time point. Cryogenic quenching and vacuum sublimation is a simpler sample preparation method than full cryo-TEM examination, but this route often results in eutectic ridges.<sup>43</sup> This occurs when dissolved solutes, whose solute–water phase diagrams exhibit eutectic points

(such as sodium chloride, sodium sulphate, calcium chloride and sodium carbonate), undergo solute partitioning into ice and solute hydrates. This can happen during the slower vacuum sublimation step or the more rapid initial freezing process (where the severity may scale with ice thickness) and can severely complicate observations of species that had actually crystallised in the original solution (Figure S8A). Such solute partitioning was not observed in cryo-TEM here, where imaging was conducted in thin regions of vitreous ice in the centre of the grid.

We therefore recommend cryogenic quenching and cryo-TEM examination of vitrified samples as the most reliable method for observing the early stages of crystallisation processes. However, even cryo-TEM analysis has some limitations, in the most part due to ice contamination. It is very common that frost, crystalline ice and frozen ethane will be present on a cryo-TEM grid and this has been shown often in the literature.<sup>44–46</sup> Such contamination is difficult to eradicate and, in the case of studying the early stages of crystallisation, can make it difficult to distinguish ‘real’ species from ice/frost/ethane. Therefore, we suggest that cryo-TEM imaging is carried out where possible in conjunction with at least one other analytical TEM technique such as SAED or EDX to confirm that species are not just contaminants caused during the freezing and subsequent loading process. Looking to the future the use of new cryogenic freezing methods, which offer improved time resolution and potentially eliminate the segregation of species at the air–water interface, should allow further improvements in the methods used to prepare specimens for cryo-TEM.<sup>47–49</sup>

## 4 | CONCLUSIONS

This work has revealed that commonly used sample preparation methods for TEM and SEM can produce artefacts in the crystallising solutions analysed, and result in erroneous interpretations of the crystallisation mechanism. This alone requires a re-interpretation of many existing results in the literature. We strongly recommend the use of cryogenic quenching of crystallising solutions and the examination of vitrified samples using cryo-TEM. Use of this approach suggests that bassanite is not an intermediate in the direct crystallisation of gypsum from bulk solution. Samples prepared by cryogenic quenching followed by vacuum sublimation of the vitreous ice possibly hint at the presence of binodal liquid–liquid de-mixing in solution prior to gypsum formation, although further study is required to confirm this. Furthermore, for the case of calcium carbonate, the cryogenic sample preparation method and examination by cryo-TEM suggests the

presence of binodal de-mixing and the formation of dense liquid phases prior to the precipitation of ACC and its subsequent transformation to crystalline polymorphs if the solution concentration exceeds the spinodal limit. Note further work is required to investigate calcium carbonate solutions below the spinodal limit.

Ultimately, this work emphasises the need to consider carefully EM sample preparation when designing experiments to study early stages of chemical reactions and crystallisation in order to avoid any artefacts and determine true reaction mechanisms.

## 5 | MATERIALS AND METHODS

### 5.1 | Synthesis of the precursor solutions

Calcium sulphate: equal volumes of aqueous 100 mM  $\text{CaCl}_2$  and 100 mM  $\text{Na}_2\text{SO}_4$  were prepared and then mixed to create a 50 mM calcium sulphate solution and initiate crystallisation. Samples were taken at various timepoints (5, 20, 60 and 120 min). 100 mM solutions of calcium sulphate were also studied. For reference, the solubility of gypsum in water at room temperature is approximately 15 mM.

Calcium carbonate: equal volumes of aqueous 9 mM  $\text{CaCl}_2$  and 9 mM  $\text{Na}_2\text{CO}_3$  were prepared and then mixed to initiate crystallisation. Samples of this 4.5 mM calcium carbonate solution were taken at various timepoints (5, 15 and 40 min). For reference, the solubility of calcite in water at room temperature is approximately 0.1 mM.

### 5.2 | Sample preparation for electron microscopy

Samples were prepared for TEM examination in the following ways:

1. Samples prepared by air drying: ( $\text{Ar}/\text{O}_2$ ) plasma-treated continuous carbon TEM grids were placed in a Petri dish and after an allotted time period, the grids were removed from the crystallising solution, extra water was blotted off by touching the side of the grids on a filter paper and finally dried in ambient air at room temperature.
2. Samples prepared by vacuum filtration: as for air drying, except that the TEM grids were removed from the Petri dish and immediately placed on a filter paper in a vacuum-filtration (Buchner) funnel to dry.
3. Samples prepared by chemical quenching: as for air drying, except that the TEM grids were removed from the Petri dish and submerged in ethanol to quench the crys-

tallisation process before blotting with a filter paper and drying at room temperature.

4. Samples prepared by cryo-quenching and vacuum sublimation: a 3  $\mu\text{L}$  droplet of the crystallising solution was transferred onto a plasma-treated continuous TEM grid after set times. This was then blotted for 5 s and the grid was rapidly plunged into liquid ethane using an FEI Vitrobot®, which causes the entire specimen to become fixed in its hydrated state with any water rapidly transforming to vitreous ice. Grids were then transferred into a vacuum desiccator to allow a controlled sublimation of the vitreous ice.<sup>50</sup>
5. Samples prepared by cryo-quenching and examination by cryo-TEM: As for cryo-quenching and vacuum sublimation, except that Quantifoil TEM grids (EM resolutions) were used and vitrified samples were stored under liquid nitrogen before examination by cryo-TEM.

Sample grids were examined using a number of different microscopes: a SU8230 Hitachi SEM, an FEI Tecnai G2 F20 X-TWIN operating at 200 kV and an FEI Titan3 Themis 300: X-FEG operating at 300 kV equipped with an FEI Super-X energy dispersive X-ray (EDX) system and a Gatan OneView CCD. A ca. 1.4 Å probe was formed for STEM with an estimated convergence semi-angle of ca. 10 mrad (limited by the second smallest C3 aperture) and a probe current of up to 150 pA for STEM (as measured by the dose metre on the flu cam, calibrated using a Faraday cup). Cryo-TEM was performed on both the Titan Themis with a Gatan Cryo-holder and also an FEI Titan Krios G3i, X-FEG and autoloader operating at 300 kV and equipped with an FEI Ceta and FEI Falcon E3C direct electron detectors. In order to reduce the charging of the samples, all of the SEM samples were coated with a thin layer of iridium prior to SEM analysis. Particle sizes (maximum Feret diameters) were measured directly from SEM and TEM images and typically included measurements of >20 particles, uncertainties are given as the standard deviation.

CIF files used for fitting SAED patterns were as follows:

Bassanite – Bullirano P, Maras A, Meloni S, Caminiti R; *European Journal of Mineralogy* 13 (2001) 985–993 \_database\_code\_amcsd 0006909

Gypsum – Schofield P F, Knight K S, Stretton I C, *American Mineralogist* 81 (1996) 847–851 \_database\_code\_amcsd 0001807

Calcite – Markgraf S A, Reeder R J, *American Mineralogist* 70 (1985) 590–600 \_database\_code\_amcsd 0000985

## ACKNOWLEDGEMENTS

We acknowledge the Engineering and Physical Sciences Research Council (EPSRC) for funding via Programme grant number EP/R018820/1 which funds the 'Crystallisa-



tion in the Real World' Consortium. We also acknowledge very useful discussions with Aaron Finney who was part of this consortium. The FEI Titan Krios microscope used in this work was funded by the University of Leeds (UoL ABSL award) and Wellcome (108466/Z/15/Z), with direct electron detector (Q2 2021) upgrades funded by Wellcome 221524/Z/20/Z. The FEI Titan Themis microscope used in this work was supported by the EPSRC under grant EP/M028143/1.

## ORCID

Martha Ilett  <https://orcid.org/0000-0002-3111-1585>

## REFERENCES

- Byard, S. J., Jackson, S. L., Smail, A., & Bauer, M., Apperley, D. C. (2005). Studies on the crystallinity of a pharmaceutical development drug substance. *Journal of Pharmaceutical Sciences*, 94(6), 1321–1335. <https://doi.org/10.1002/jps.20328>
- Ryu, J., Ku, S. H., Lee, H., & Park, C. B. (2010). Mussel-inspired polydopamine coating as a universal route to hydroxyapatite crystallization. *Advanced Functional Materials*, 20(13), 2132–2139. <https://doi.org/10.1002/adfm.200902347>
- S'ari, M., Cattle, J., Hondow, N., Brydson, R., & Brown, A. (2019). Low dose scanning transmission electron microscopy of organic crystals by scanning moiré fringes. *Micron*, 120, 1–9. <https://doi.org/10.1016/j.micron.2019.01.014>
- Coe, F. L., Evan, A., & Worcester, E. (2005). Kidney stone disease. *The Journal of Clinical Investigation*, 115(10), 2598–2608. <https://doi.org/10.1172/JCI26662>
- Elert, K., Bel-Anzué, P., & Burgos-Ruiz, M. (2023). Influence of calcination temperature on hydration behavior, strength, and weathering resistance of traditional gypsum plaster. *Construction and Building Materials*, 367, 130361. <https://doi.org/10.1016/j.conbuildmat.2023.130361>
- Karthika, S., Radhakrishnan, T. K., & Kalaichelvi, P. (2016). A review of classical and nonclassical nucleation theories. *Crystal Growth & Design*, 16(11), 6663–6681. <https://doi.org/10.1021/acs.cgd.6b00794>
- Guo, C., Wang, J., Li, J., Wang, Z., & Tang, S. (2016). Kinetic pathways and mechanisms of two-step nucleation in crystallization. *The Journal of Physical Chemistry Letters*, 7(24), 5008–5014. <https://doi.org/10.1021/acs.jpclett.6b02276>
- Vekilov, P. G. (2010). Nucleation. *Crystal Growth & Design*, 10(12), 5007–5019. <https://doi.org/10.1021/cg1011633> PubMed
- Vekilov, P. G. (2010). The two-step mechanism of nucleation of crystals in solution. *Nanoscale*, 2(11), 2346–2357. <https://doi.org/10.1039/C0NR00628A>
- Erdemir, D., Lee, A. Y., & Myerson, A. S. (2009). Nucleation of crystals from solution: Classical and two-step models. *Accounts of Chemical Research*, 42(5), 621–629. <https://doi.org/10.1021/ar800217x>
- Jin, B., Liu, Z., & Tang, R. (2020). Recent experimental explorations of non-classical nucleation. *CrystEngComm*, 22(24), 4057–4073. <https://doi.org/10.1039/D0CE00480D>
- Michen, B., Geers, C., Vanhecke, D., Endes, C., Rothen-Rutishauser, B., Balog, S., & Petri-Fink, A. (2015). Avoiding drying-artifacts in transmission electron microscopy: Characterizing the size and colloidal state of nanoparticles. *Scientific Reports*, 5(1), 9793. <https://doi.org/10.1038/srep09793>
- Jia, C., Zhu, G., Legg, B. A., Guan, B., & De Yoreo, J. J. (2022). Bassanite grows along distinct coexisting pathways and provides a low energy interface for gypsum nucleation. *Crystal Growth & Design*, 22(11), 6582–6587. <https://doi.org/10.1021/acs.cgd.2c00794>
- Sand, K. K., Rodriguez-Blanco, J. D., Makovicky, E., Benning, L. G., & Stipp, S. L. S. (2012). Crystallization of CaCO<sub>3</sub> in water-alcohol mixtures: Spherulitic growth, polymorph stabilization, and morphology change. *Crystal Growth & Design*, 12(2), 842–853. <https://doi.org/10.1021/cg2012342>
- Ilett, M. A.-O., Freeman, H. M., Aslam, Z., Galloway, J. M., Klebl, D. P., Muench, S. P., McPherson, I. J., Cespedes, O., Kim, Y. Y., Meldrum, F. C., Yeandel, S. R., Freeman, C. L., Harding, J. H., & Brydson, R. M. D. (2022). Evaluation of correlated studies using liquid cell and cryo-transmission electron microscopy: Hydration of calcium sulphate and the phase transformation pathways of bassanite to gypsum. *Journal of Microscopy*, 288(3), 155–168.
- Ilett, M., S'ari, M., Freeman, H., Aslam, Z., Koniuch, N., Afzali, M., Cattle, J., Hooley, R., Roncal-Herrero, T., Collins, S. M., Hondow, N., Brown, A., & Brydson, R. (2020). Analysis of complex, beam-sensitive materials by transmission electron microscopy and associated techniques. *Philosophical Transactions of the Royal Society A: Mathematical, Physical and Engineering Sciences*, 378(2186), 20190601. <https://doi.org/10.1098/rsta.2019.0601>
- Elliot, A. J., & Bartels, D. M. (2009). The reaction set, rate constants and g-values for the simulation of the radiolysis of light water over the range 20 to 350 deg C based on information available in 2008; AECL-153-127160-450-001. Canada. [http://inis.iaea.org/search/search.aspx?orig\\_q=RN:41057263](http://inis.iaea.org/search/search.aspx?orig_q=RN:41057263)
- Speedy, R. J., & Angell, C. A. (1976). Isothermal compressibility of supercooled water and evidence for a thermodynamic singularity at –45°C. *The Journal of Chemical Physics*, 65(3), 851–858. <https://doi.org/10.1063/1.433153>
- Van Driessche, A. E. S., Stawski, T. M., & Kellermeier, M. (2019). Calcium sulfate precipitation pathways in natural and engineered environments. *Chemical Geology*, 530, 119274. <https://doi.org/10.1016/j.chemgeo.2019.119274>
- Anduix-Canto, C., Levenstein, M. A., Kim, Y.-Y., Godinho, J. R. A., Kulak, A. N., Niño, C. G., Withers, P. J., Wright, J. P., Kapur, N., Christenson, H. K., & Meldrum, F. C. (2021). Exploiting confinement to study the crystallization pathway of calcium sulfate. *Advanced Functional Materials*, 31(50), 2107312. <https://doi.org/10.1002/adfm.202107312>
- Galloway, J. M., Aslam, Z. P., Yeandel, S. R., Kulak, A., Ilett, M. A., Kim, Y.-Y., Bejarano-Villafuerte, A., Pokroy, B., Drummond-Brydson, R. M., Freeman, C. L., Harding, J. H., Kapur, N., & Meldrum, F. C. (2023). Electron transparent nanotubes reveal crystallization pathways in confinement. *Chemical Science*, 14(24), 6705–6715. <https://doi.org/10.1039/D3SC00869J>
- Tritschler, U., Kellermeier, M., Debus, C., & Kempter, A., Colfen, H. (2015). A simple strategy for the synthesis of well-defined bassanite nanorods. *Crystengcomm*, 17(20), 3772–3776. <https://doi.org/10.1039/c5ce00519a>
- Wang, Y. W., Kim, Y. Y., Christenson, H. K., & Meldrum, F. C. (2012). A new precipitation pathway for calcium sulfate dihydrate (gypsum) via amorphous and hemihydrate intermediates.

- Chemical Communications*, 48(4), 504–506. <https://doi.org/10.1039/c1cc14210k>
24. Jones, F. (2012). Infrared investigation of barite and gypsum crystallization: Evidence for an amorphous to crystalline transition. *Crystengcomm*, 14(24), 8374–8381. <https://doi.org/10.1039/c2ce25918d>
  25. He, K., Nie, A. M., Yuan, Y. F., Ghodsi, S. M., Song, B. A., Firlar, E., Lu, J., Lu, Y. P., Shokuhfar, T., Megaridis, C. M., & Shahbazian-Yassar, R. (2018). In situ transmission electron microscopy explores a new nanoscale pathway for direct gypsum formation in aqueous solution. *Acs Applied Nano Materials*, 1(10), 5430–5440. <https://doi.org/10.1021/acsanm.8b00739>
  26. Stawski, T. M., van Driessche, A. E. S., Ossorio, M., Rodriguez-Blanco, J. D., Besselink, R., & Benning, L. G. (2016). Formation of calcium sulfate through the aggregation of sub-3 nanometre primary species. *Nature Communications*, 7, 11177. <https://doi.org/10.1038/ncomms11177>
  27. Van Driessche, A. E. S., Benning, L. G., Rodriguez-Blanco, J. D., Ossorio, M., Bots, P., & Garcia-Ruiz, J. M. (2012). The role and implications of bassanite as a stable precursor phase to gypsum precipitation. *Science*, 336(6077), 69–72. <https://doi.org/10.1126/science.1215648>
  28. Kralj, D., & Brečević, L. (1995). Dissolution kinetics and solubility of calcium carbonate monohydrate. *Colloids and Surfaces A: Physicochemical and Engineering Aspects*, 96(3), 287–293. [https://doi.org/10.1016/0927-7757\(94\)03063-6](https://doi.org/10.1016/0927-7757(94)03063-6)
  29. Aydinol, M. K., Mantese, J. V., & Alpay, S. P. (2007). A comparative ab initio study of the ferroelectric behaviour in KNO<sub>3</sub> and CaCO<sub>3</sub>. *Journal of Physics: Condensed Matter*, 19(49), 496210. <https://doi.org/10.1088/0953-8984/19/49/496210>
  30. Christy, A. G. (2017). A review of the structures of vaterite: The impossible, the possible, and the likely. *Crystal Growth & Design*, 17(6), 3567–3578. <https://doi.org/10.1021/acs.cgd.7b00481>
  31. Pouget, E. M., Bomans, P. H. H., Dey, A., Frederik, P. M., de With, G., & Sommerdijk, N. A. J. M. (2010). The development of morphology and structure in hexagonal vaterite. *Journal of the American Chemical Society*, 132(33), 11560–11565. <https://doi.org/10.1021/ja102439r>
  32. Gower, L. B. (2008). Biomimetic model systems for investigating the amorphous precursor pathway and its role in biomineralization. *Chemical Reviews*, 108(11), 4551–4627. <https://doi.org/10.1021/cr800443h>
  33. Rodriguez-Blanco, J. D., Shaw, S., & Benning, L. G. (2011). The kinetics and mechanisms of amorphous calcium carbonate (ACC) crystallization to calcite, viavaterite. *Nanoscale*, 3(1), 265–271. <https://doi.org/10.1039/C0NR00589D>
  34. Gebauer, D., & Cölfen, H. (2011). Prenucleation clusters and non-classical nucleation. *Nano Today*, 6(6), 564–584. <https://doi.org/10.1016/j.nantod.2011.10.005>
  35. Sebastiani, F., Wolf, S. L. P., Born, B., Luong, T. Q., Cölfen, H., Gebauer, D., & Havenith, M. (2017). Water dynamics from THz spectroscopy reveal the locus of a liquid–liquid binodal limit in aqueous CaCO<sub>3</sub> solutions. *Angewandte Chemie International Edition*, 56(2), 490–495. <https://doi.org/10.1002/anie.201610554>
  36. Yang, L.-X., Meng, Y.-F., Yin, P., Yang, Y.-X., Tang, Y.-Y., & Qin, L.-F. (2011). Shape control synthesis of low-dimensional calcium sulfate. *Bulletin of Materials Science*, 34(2), 233–237. <https://doi.org/10.1007/s12034-011-0078-4>
  37. Gebauer, D., Kellermeier, M., Gale, J. D., & Bergström, L., Cölfen, H. (2014). Pre-nucleation clusters as solute precursors in crystallisation. *Chemical Society Reviews*, 43(7), 2348–2371. <https://doi.org/10.1039/C3CS60451A>
  38. Smeets, P. J. M., Finney, A. R., Habraken, W., Nudelman, F., Friedrich, H., Laven, J., De Yoreo, J. J., Rodger, P. M., & Sommerdijk, N. (2017). A classical view on nonclassical nucleation. *PNAS*, 114(38), E7882–E7890.
  39. Zou, Z., Habraken, W. J. E. M., Bertinetti, L., Politi, Y., Gal, A., Weiner, S., Addadi, L., & Fratzl, P. (2017). On the phase diagram of calcium carbonate solutions. *Advanced Materials Interfaces*, 4(1), 1600076. <https://doi.org/10.1002/admi.201600076>
  40. Manoli, F., & Dalas, E. (2000). Spontaneous precipitation of calcium carbonate in the presence of ethanol, isopropanol and diethylene glycol. *Journal of Crystal Growth*, 218(2), 359–364. [https://doi.org/10.1016/S0022-0248\(00\)00560-1](https://doi.org/10.1016/S0022-0248(00)00560-1)
  41. Walker, J. M., Marzec, B., & Nudelman, F. (2017). Solid-state transformation of amorphous calcium carbonate to aragonite captured by cryoTEM. *Angewandte Chemie International Edition*, 56(39), 11740–11743. <https://doi.org/10.1002/anie.201703158>
  42. Farhadi-Khouzani, M., Chevrier, D. M., Zhang, P., Hedin, N., & Gebauer, D. (2016). Water as the key to proto-aragonite amorphous CaCO<sub>3</sub>. *Angewandte Chemie International Edition*, 55(28), 8117–8120. <https://doi.org/10.1002/anie.201603176>
  43. Wergin, W. P., & Erbe, E. F. (1992). Techniques for obtaining and observing complementary images with a low-temperature field emission SEM and subsequent comparison of the identical cells in freeze-etch replicas viewed with a TEM. *Scanning*, 14(1), 17–30. <https://doi.org/10.1002/sca.4950140105>
  44. Burrows, N. D., & Penn, R. L. (2013). Cryogenic transmission electron microscopy: Aqueous suspensions of nanoscale objects. *Microscopy and Microanalysis*, 19(6), 1542–1553. <https://doi.org/10.1017/s1431927613013354>
  45. Grassucci, R. A., Taylor, D. J., & Frank, J. (2007). Preparation of macromolecular complexes for cryo-electron microscopy. *Nature Protocols*, 2(12), 3239–3246. <https://doi.org/10.1038/nprot.2007.452>
  46. Thompson, R. F., Walker, M., Siebert, C. A., Muench, S. P., & Ranson, N. A. (2016). An introduction to sample preparation and imaging by cryo-electron microscopy for structural biology. *Methods*, 100, 3–15. <https://doi.org/10.1016/j.ymeth.2016.02.017>
  47. Klebl, D. P., Monteiro, D. C. F., Kontziampasis, D., Kopf, F., Sobott, F., White, H. D., Trebbin, M., & Muench, S. P. (2020). Sample deposition onto cryo-EM grids: From sprays to jets and back. *Acta Crystallographica Section D*, 76(4), 340–349. <https://doi.org/10.1107/S20597983200002958>
  48. Klebl, D. P., White, H. D., Sobott, F., & Muench, S. P. (2021). On-grid and in-flow mixing for time-resolved cryo-EM. *Acta Crystallographica Section D*, 1(77), 1233–1240.
  49. Kontziampasis, D., Klebl, D. P., Iadanza, M. G., Scarff, C. A., Kopf, F., Sobott, F., Monteiro, D. C. F., Trebbin, M., Muench, S. P., & White, H. D. (2019). A cryo-EM grid preparation device for time-resolved structural studies. *IUCrJ*, 6(Pt 6), 1024–1031. <https://doi.org/10.1107/s2052252519011345>
  50. Hondow, N., Brydson, R., Wang, P., Holton, M. D., Brown, M. R., Rees, P., Summers, H. D., & Brown, A. (2012). Quantitative characterization of nanoparticle agglomeration within biologi-

cal media. *Journal of Nanoparticle Research*, 14(7), 977. <https://doi.org/10.1007/s11051-012-0977-3>

## SUPPORTING INFORMATION

Additional supporting information can be found online in the Supporting Information section at the end of this article.

**How to cite this article:** Ilett, M., Afzali, M., Abdulkarim, B., Aslam, Z., Foster, S., Burgos-Ruiz, M., Kim, Y.-Y., Meldrum, F., & Drummond-Brydson, R. M. (2024). Studying crystallisation processes using electron microscopy: The importance of sample preparation. *Journal of Microscopy*, 295, 243–256. <https://doi.org/10.1111/jmi.13300>